Resolution enhancement of digital laser scanning fluorescence microscopy with a dual-lens optical pickup head

Rung-Ywan Tsai, Jung-Po Chen, Yuan-Chin Lee, Hung-Chih Chiang, Tai-Ting Huang, Chun-Chieh Huang, Chih-Ming Cheng, Chung-Ta Cheng, et al.

Optical Review

ISSN 1340-6000
Volume 23
Number 5

Opt Rev (2016) 23:817-823
DOI 10.1007/s10043-016-0246-2

Springer

Opt Rev (2016) 23:817–823
DOI 10.1007/s10043-016-0246-2

SPECIAL SECTION: REGULAR PAPER

The 10th International Conference on Optics-Photonics Design & Fabrication (ODF'16), Weingarten, Germany

Resolution enhancement of digital laser scanning fluorescence microscopy with a dual-lens optical pickup head

Rung-Ywan Tsai[1] · Jung-Po Chen[1] · Yuan-Chin Lee[2] · Hung-Chih Chiang[2] · Tai-Ting Huang[2] · Chun-Chieh Huang[2] · Chih-Ming Cheng[2] · Chung-Ta Cheng[2] · Feng-Hsiang Lo[1] · Golden Tiao[1]

Received: 15 April 2016 / Accepted: 5 July 2016 / Published online: 21 July 2016

Abstract The resolution of the cell fluorescence image captured by a digital laser scanning microscopy with a modified dual-lens BD-ROM optical pickup head is enhanced by image registration and double sample frequency. A dual objective lens of red (655 nm) and blue (405 or 488 nm) laser sources with numerical apertures of 0.6 and 0.85 is used for sample focusing and position tracking and cell fluorescence image capturing, respectively. The image registration and capturing frequency are based on the address-coded patterns of a sample slide. The address-coded patterns are designed as a string of binary code, which comprises a plurality of base-straight lands and grooves and data-straight grooves. The widths of the base-straight lands, base-straight grooves, and data-straight grooves are 0.38, 0.38, and 0.76 μm, respectively. The numbers of sample signals in the *x*-direction are measured at every intersection point by intersecting the base intensity of the push–pull signal of the address-coded patterns, which has a minimum spacing of 0.38 μm. After taking a double sample frequency, the resolution of the measured cell fluorescence image is enhanced from 0.38 μm to the diffraction limit of the objective lens.

Keywords Fluorescence image · Resolution · Digital laser scanning microscopy · Address-coded pattern · Optical pickup head

✉ Rung-Ywan Tsai
ry.tsai@caduceus.com.tw

[1] Caduceus Biomedical Inc., Hsinchu 310, Taiwan

[2] Industrial Technology Research Institute, Biomedical Technology and Device Research Laboratories, Hsinchu 310, Taiwan

1 Introduction

Digital laser scanning fluorescence microscopy (DLSM) has been popularly used in life sciences for microstructural observations of species at the molecular level, which is essential for the rapid and accurate diagnosis and monitoring of medical diseases [1–3]. However, the commercial DLSM is bulky, expensive, and inconvenient for a number of potential applications, including in situ monitoring of cell growth dynamics in cell culture chambers [4].

We have developed a compact, position-addressable, and cost-effective DLSM for cell fluorescence image capturing, as shown in Fig. 1 [5, 6]. The DLSM system was modified from a commercial Blu-ray read-only memory (BD-ROM) optical pickup head (OPH) module. The OPH module contained a dual objective lens of blue (405 nm) and red (655 nm) laser sources; one was for BD optics and the other one was for digital video disk (DVD) optics, respectively. We used the blue and red lasers as light sources for cell fluorescence image capturing and position recognition, respectively. A specially designed sample slide of 25.4 × 76.2 mm^2 contained 8 wells and each well contained two areas. One area of 4.0 × 7.14 mm^2 was the sample area for cell sample loading and the other area of 3.08 × 7.14 mm^2 was address-patterned area for address recognition. The blue laser beam was focused on the sample area and was used for fluorescent excitation and image capturing, whereas the red laser beam was focused on the address-patterned area and was used for address recognition and dynamic focusing. Therefore, the obtained cell image or the signal of each sampling area had an accurate corresponding address.

Several advantages were expected for the position-addressable DLSM system, such as to form a large-format cell image by stitching the small-format images adjacent to

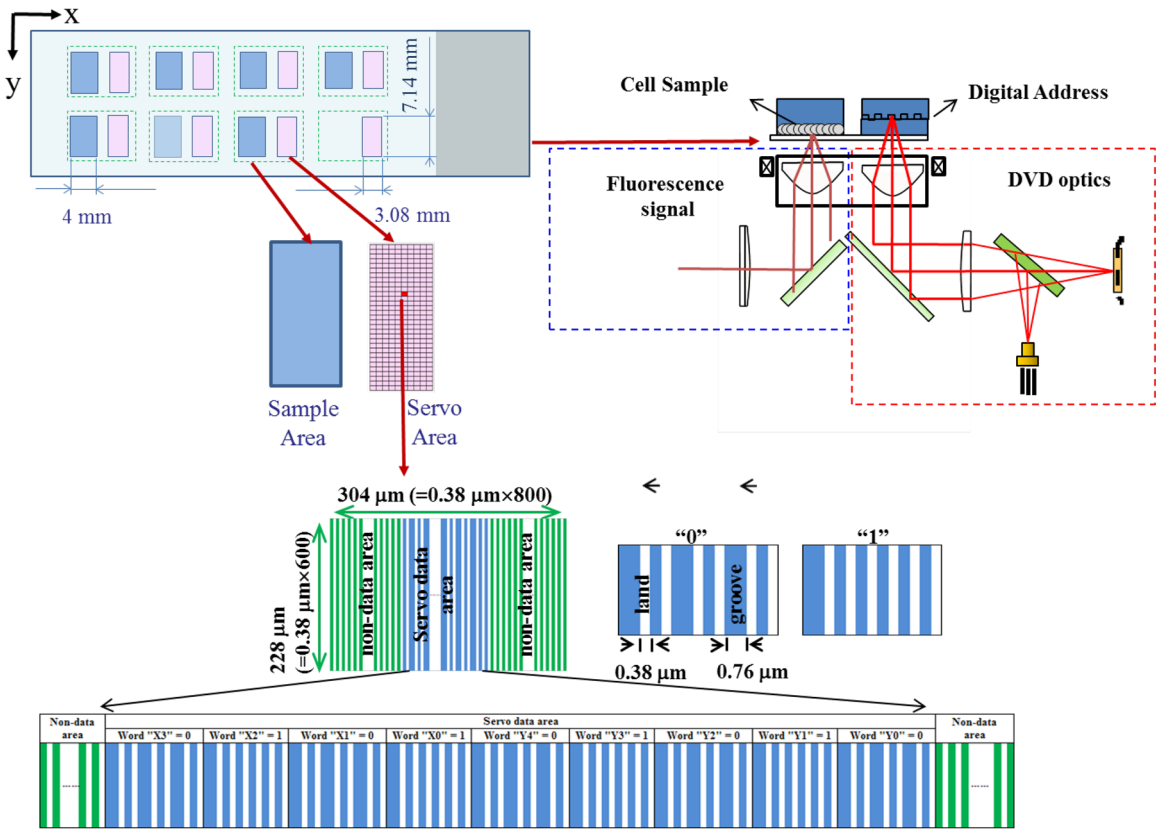

Fig. 1 Optical layout of the DLSM system, the configuration of the sample slide, and the microstructure of the servo code area of sector [5, 10]

each other [5], to increase the signal-to-noise ratio of the image by scanning the same address image multiple times [7, 8], to obtain the three-dimensional image by stacking images measured at different z-sections at the same *x*–*y* position [6, 9–11], to capture the multicolor fluorescence image of the same cell using the different dyes and excitation lasers [12–14], and to monitor the cell growth and evolution with the time [13–15].

The address-coded area of the sample slide was divided into serval sectors, as shown in Fig. 1. Each sector had its unique binary-coded pattern comprising a plurality of base-straight lands and grooves and data-straight grooves. The fluorescence signal of the sample was taken at the base value (when PP signal is zero) across the push–pull (PP) signal when position-recognition laser beam swung across the address-coded patterns of the sector. The number of the "sample signal" (pixel) represents the length of the sector image. The image specification of each sector was originally set to 800 × 600 pixels (SVGA format) in the *x*- and *y*-directions. However, the measured coded pattern and the corresponding number of pixels in our previous report were different from sector to sector. [5] The variations of pixel numbers between different sectors could be up to 14 pixels. Meanwhile, the resolution of the captured cell fluorescence image was 0.38 μm, which was determined by the minimum feature size of the address-coded pattern. However, the optical resolutions of 405 and 488 nm laser beams using an objective lens with numerical aperture (NA) of 0.85 were 0.29 and 0.35 μm, respectively, which were smaller than 0.38 μm of the image captured by our DLSM [16].

In this study, we developed an image registration and capturing method to correct the lost pixels of the sector due to the different address-coded patterns of each sector. After correction, every sector has the same pixel numbers of 800 × 600 with the resolution of 0.38 μm. We also used the double sample frequency to increase the pixel numbers of the sector from 800 × 600 to 1600 × 1200, and thus, the resolution of every pixel was enhanced up to the diffraction limit of the image capturing objective lens.

2 Experiment

The fluorescence cell image was taken by the DLSM system modified from commercial Blu-ray BD-ROM (Sanyo SF-BD412) optical pickup head (OPH) [5]. An injected plastic sample slide of 25.4 × 76.2 mm^2 contained sample areas and address-coded areas was used for sample holding and address coding, respectively. The address-coded area with the dimension of 7.14 × 3.08 mm^2 was divided into

310 sectors, with 10 sectors in the x-direction and 31 sectors in the y-direction. Each sector had its own address-coded pattern. The pattern of a sector comprised one servo data area and two non-data areas (Fig. 1). The microstructure of the non-data areas comprised a plurality of base-straight lands and grooves with an equal width of 0.38 μm, and that of the servo data area had a binary code comprising a plurality of base-straight lands and grooves and data-straight grooves. The width of the data-straight groove was 0.76 μm. The boundary of each sector was confined by two data-straight grooves in the x-direction. The image specification of each sector was set to 800 × 600 pixels (SVGA format) in the x- and y-directions. Because the resolution of each pixel was controlled at 0.38 μm, the entire area of each sector was 304 × 228 μm^2. A string of binary code comprising nine digital data points was used to describe the sector number. The first four digits were used to record the sector number (0–9) in the x-direction, and the last five digits were used to record the sector number (0–30) in the y-direction. Therefore, the sector number could be expressed as (x, y). The pattern of digital data "0" comprised three data-straight grooves, three base-straight grooves, and six base-straight lands, and that of digital data "1" comprised one data-straight groove, five base-straight grooves, and six base-straight lands.

A swing frequency of 40 Hz for the voice coil motor (VCM), with a displacement over 304 μm across a sector in the x-direction, was adopted in the address tracking. Meanwhile, the movement of the sample slide along the y-direction was controlled by stepping motor. Therefore, 80 pixels along the y-direction were taken in 1 s and the total capturing time was 7.5 s for 600 pixels in one sector with height of 228 μm. According to the pattern of the binary code, the sample signal was taken at the base value across the PP signal when the VCM swung across the sector (Fig. 2a). Although the data-straight groove had the width (0.76 μm) twice of that of base-straight lands and grooves (0.38 μm), the captured number of sample signal (pixel) was counted as one but not two. Therefore, it causes a loss of a pixel of sample signal for one data-straight groove. Taken sector [5, 10] as an example (Fig. 1), the string of binary code (010101010) comprised 19 data-straight grooves. Therefore, the total number of captured sample signals in this sector was 781 pixels and 19 pixels were lost in the x-direction. Different sectors had different numbers of data-straight grooves, which caused the different numbers of lost pixels in the x-direction. In our previous method, the lost pixels were set as blank signals and added at the end of the scanned image [5]. In here, we used a more accurate method based on the logical OR operator to compensate the lost image (Fig. 2b). From the simulated PP signal, a threshold intensity (yellow dashed line in Fig. 2a) was used to distinguish the data-straight groove and the base-straight groove. When the intensity was higher than the threshold value, a large signal was obtained from the data-straight groove. When the intensity was lower than the threshold value but higher than the base value (green solid line in Fig. 2a), a small signal was contributed from the base-straight groove. For every base-straight groove, one pixel was counted, whereas two pixels were sequentially counted for every data-straight groove by the field programmable gate array (FPGA). Therefore, every sector had the same image pixels of 800 × 600 in the $x \times y$ directions with the resolution of 0.38 μm. Similarly, the pixel numbers of the captured image in the $x \times y$ directions could be increased from 800 × 600 pixels to 1600 × 1200 pixels by doubling the sample frequency. That means two pixels were sequentially counted for every base-straight groove and four pixels were counted for every data-straight groove by the field programmable gate array (FPGA). The theoretical image resolution was then enhanced from 0.38 μm up to 0.19 μm (half of 0.38 μm) within the same sector area of 304 × 228 μm^2.

Monkey-derived kidney epithelial (VERO) cells were plated in antibiotic-free Alpha Modifications Minimum Essential Medium in 5 % phosphate-buffered saline (PBS). The cell samples were stained with Alexa Fluor® 488 phalloidin (30 U/mL) (Molecular Probes, Oregon, USA). Another sample of tissue fiber was stained with phalloidin CF™ 405 (50 U/mL) (Biotium, CA, USA). The images of the VERO cell and tissue fibers were captured by DLSM with excitation lasers of 488 and 405 nm, respectively, and an objective lens of NA 0.85. A high-sensitivity photomultiplier tube (PMT, Hamamatsu H10723-210) based on photoelectric effect was used to measure the emitted fluorescence light. The control voltage of PMT was 0.94 V, with an electron multiplier (gain) of 1.13 × 10^6. The surface morphology and topography of sample slides were analyzed by field emission scanning electron microscope (FE-SEM, HITACHI S-4800) and atomic force of microscopy (AFM, Digital Instrument DI 500), respectively.

3 Results and discussion

The plastic sample slide produced by injection molding is shown in Fig. 3a. The sample slide contains 8 wells and each well contains two areas. One area is the sample area for cell sample loading, and the other area is the address-coded area with the patterned land-groove structures. The microstructure of the injected sample slide with the land-groove morphologies of (101) barcode is clearly shown in Fig. 3b. The widths of base-straight lands and grooves are 0.38 μm, and the depth of the base-straight groove is ~65 nm as measured by AFM (Fig. 3c). The VERO cell

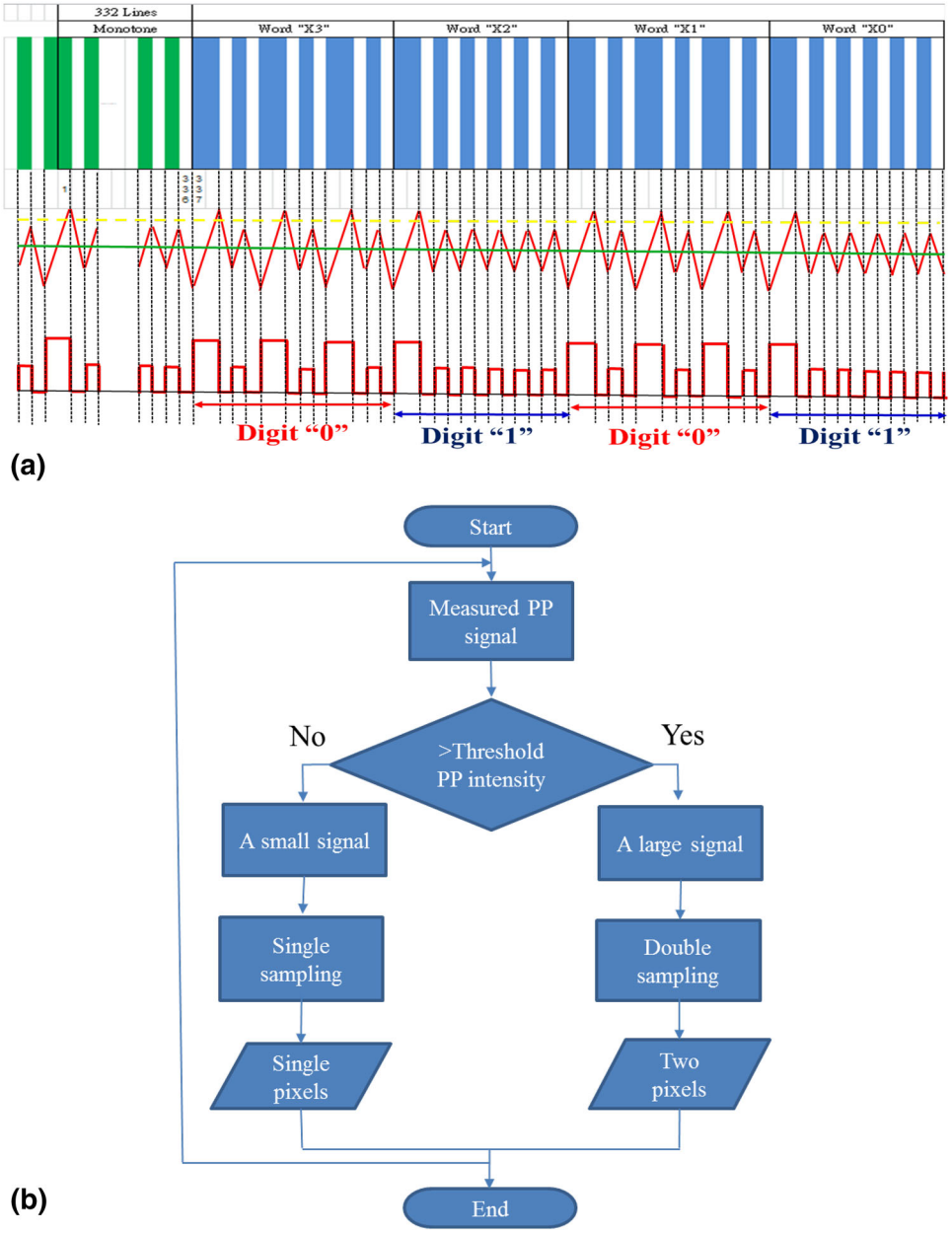

Fig. 2 **a** Simulated (*middle*) and decoded (*bottom*) PP signals of the servo code area (*top*) in part of the sector (x, y) at $x = 5$. The *horizontal yellow dashed line* and *green solid line* in the simulated PP signal (*middle*) are the threshold intensity and base intensity, respectively. **b** Flow chart to describe the algorithm based on the logical OR operator

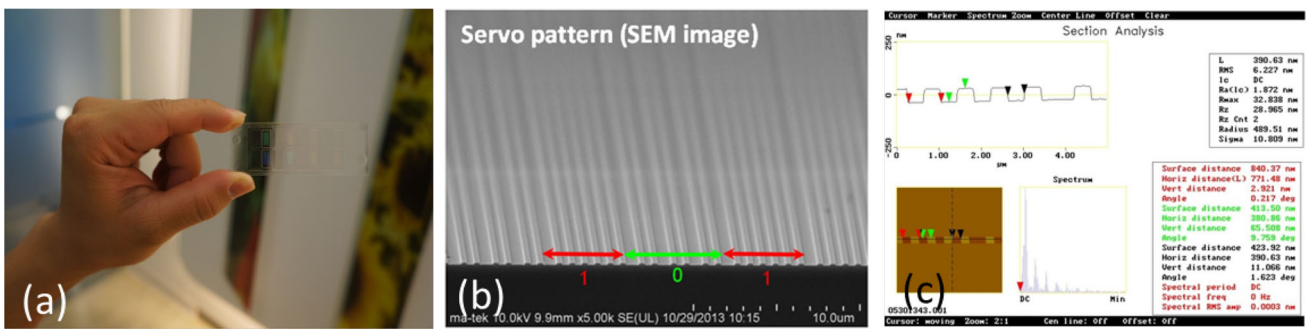

Fig. 3 **a** Injected plastic substrate, **b** and **c** SEM and AFM images of servo code area, respectively

captured by DLSM with a 488 nm excitation laser and an objective lens of NA 0.85 is shown in Fig. 4. The captured cell image without using an image registration algorithm has a periodic dark edge, which is due to the lost pixels caused by the single pixel counting of every data-straight groove (Fig. 4a, c). When the laser beam is scanned at a frequency of 40 Hz across a sector of 304 μm in the *x*-direction, the counted pixels from left end to right end (forward scan) and then from right end to left end (backward scan) of the image are less than 800 pixels and the lost pixels are set as blank signals and added at the right end and left end of the scanned images, respectively. The sample is moved at a speed time of 7.5 s along the *y*-direction to cover the sector height of 228 μm. Therefore, a sector image of 800 × 600 pixels in the $x \times y$ directions is obtained. However, the offset between the forward- and backward-scanned images along the *y*-direction causes the shuttle effect of image, as shown in the circled area of Fig. 4c. After correction by image registration algorithm, the dark-edge phenomenon of lost pixels and the shuttle image effect are completely removed, as shown in Fig. 4d. Every scanned image has an exact data of 800 pixels along the *x*-direction and is aligned quite well in *y*-direction with the resolution of 0.38 μm. No obvious shuttle effect on the scanned image is observed, indicating that image registration algorithm based on the logical OR operator can fix the lost-pixel issue of the previous method [5].

After the correction of image registration algorithm, the resolution of the VERO cell fluorescence image can be enhanced using a double sample frequency. The resolution enhancement of fluorescence images of VERO cell stained with Alexa Fluor® 488 phalloidin and captured by DLSM is shown in shown in Fig. 5. The image of the VERO cell of 1600 × 1200 measured by double frequency (Fig. 5b) is superior to that measured by single sample frequency (Fig. 5a). Moreover, the stereo effect of the image is also enhanced by increasing the pixel resolution due to the image sharpening effect [17]. Effects of image registration algorithm and double sample frequency is also applied for tissue fibers stained with phalloidin CF™ 405 and captured by DLSM with an excitation laser of 405 nm and an objective lens of NA 0.85 as shown in Fig. 6. The resolution and stereo effect of the image captured by double frequency is better than that measured by single frequency, which is even more obvious than the VERO cell image measured with a 488 nm laser and shown in Fig. 5. The theoretical resolution of the images captured by double frequency is 0.19 μm, half of 0.38 μm of single frequency. However, the optical resolutions of 405 and 488 nm laser beams using an objective lens with NA of 0.85 are 0.29 and 0.35 μm, respectively. Therefore, the resolutions of the fluorescence cell images captured by DLSM using the image registration and double sample frequency and the image enhancements can be increased up to the diffraction limits of objective lens, but cannot reach the theoretical resolution of 0.19 μm. The diffraction limit of the fluorescence cell images captured by DLSM using the laser of 405 nm is 0.29 μm, which is better than that measured by 488 nm laser beams of 0.35 μm.

4 Conclusion

A position-addressable and cost-effective DLSM system with a modified dual head OPH module of BD-ROM is used for cell fluorescence image capturing. The resolution of the captured cell fluorescence image of 800 × 600 pixels is originally determined by the minimum feature size

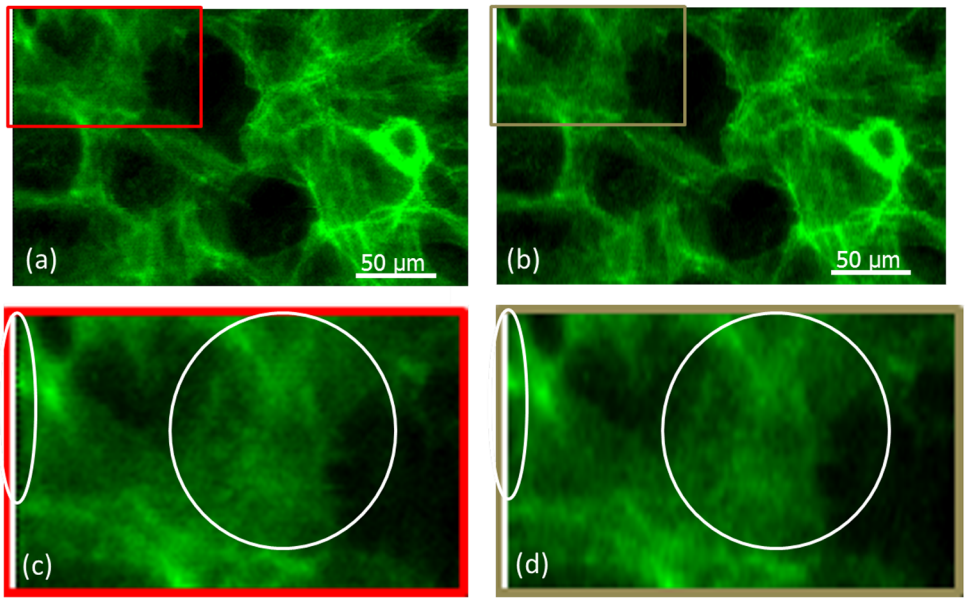

Fig. 4 Fluorescence VERO cell images stained with Alexa Fluor® 488 phalloidin and captured by DLSM **a** without and **b** with the correction of an image registration algorithm. The enlarged images of the circled areas in **a** and **b** are shown in **c** and **d**, respectively

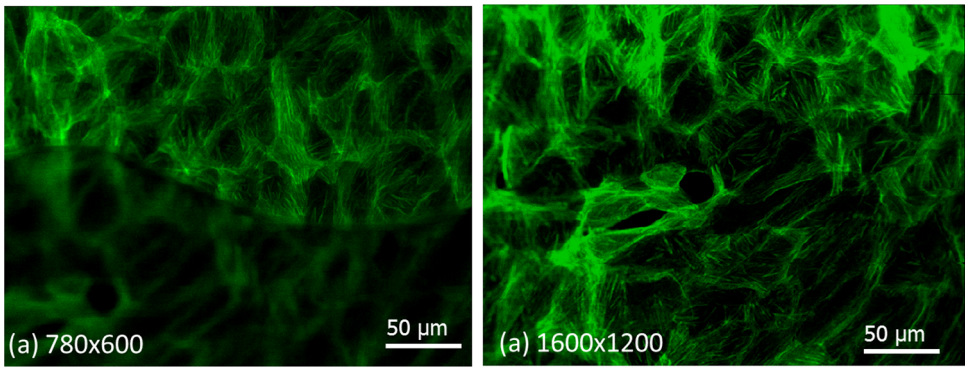

Fig. 5 Fluorescence VERO cell images stained with Alexa Fluor® 488 phalloidin and captured by DLSM with **a** single and **b** double sample frequencies

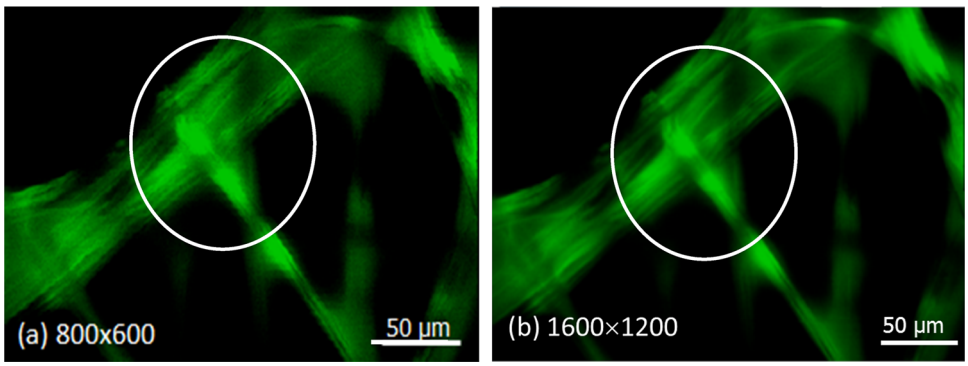

Fig. 6 Fluorescence tissue fiber images stained with fluorophore phalloidin CF™ 405 and captured by DLSM with **a** single and **b** double sample frequencies

of the address-coded pattern of 0.38 μm. With the aids of image registration and double sample frequency, the resolution of the measured cell fluorescence image of 1600 × 1200 pixels is enhanced from 0.38 μm to the diffraction limit of the objective lens.

Acknowledgments We thank Industrial Technology Research Institute for financial aid under project code F256WA1000. We are also grateful for assistance from members at the Biomedical Devices Research Laboratory in cell cultivation and preparation.

References

1. Weissleder, R., Ntziachristos, V.: Imaging of angiogenesis: from microscope to clinic. Nat. Med. **9**, 123 (2003)
2. Betzig, E., Patterson, G.H., Sougrat, R., Lindwasser, O.W., Olenych, S., Bonifacino, J.S., Lippincott-Schwartz, J., Hess, H.F.: Imaging intracellular fluorescent proteins at nanometer resolution. Science **313**, 1642 (2006)
3. Schemelleh, L., Heintzmann, R., Leonhardt, H.: A guide to super-resolution fluorescence microscopy. J. Cell Biol. **190**, 165 (2010)
4. Delaney, P.M., Harris, M.R., King, R.G.: Fiber-optic laser scanning confocal microscope suitable for fluorescence imaging. Appl. Opt. **33**, 573 (1994)
5. Tsai, R.Y., Chen, J.P., Lee, Y.C., Huang, C.C., Huang, T.T., Chiang, H.C., Cheng, C.M., Lo, F.H., Chang, S.L., Weng, K.Y., Chung, L.P., Chen, J.C., Tiao, G.: Position-addressable digital laser scanning point fluorescence microscopy with a Blu-ray disk pickup head. Biom. Opt. Express **5**, 417 (2014)
6. Tsai, R.Y., Chen, J.P., Lee, Y.C., Chiang, H.C., Cheng, C.M., Huang, C.C., Huang, T.T., Cheng, C.T., Tiao, G.: Cell depth imaging using a point laser scanning fluorescence microscopy based on an optical disk pickup head. Jpn. J. Appl. Phys. **54**, 09MD01 (2015)
7. Kim, K.H., Lee, S.Y., Kim, S., Lee, S.H., Jeong, S.G.: A new DNA chip detection mechanism using optical pick-up actuators. Microsyst. Technol. **13**, 1359 (2007)
8. De Luna, G.M.R., Breedijk, R.M.P., Brandt, R.A.J., Zeelenberg, C.H.C., de Jong, B.E., Timmermans, W., Azar, L.N., Hoebe, R.A., Strallinga, S., Manders, E.M.M.: Re-scan confocal microscopy: scanning twice for better resolution. Biomed. Opt. Express **4**, 2644 (2013)
9. Antonini, A., Liberale, C., Fellin, T.: Fluorescent layers for characterization of sectioning microscopy with coverslip-uncorrected and water immersion objectives. Opt. Express **22**, 14293 (2014)
10. Jabbour, J.M., Malik, B.H., Olsovsky, C., Cuenca, R., Cheng, S., Jo, J.A., Cheng, Y.S., Wright, J.M., Maitland, K.C.: Optical axial scanning in confocal microscopy using an electrically tunable lens. Biomed. Opt. Express **5**, 645 (2014)
11. Zipfel, W.R., Williams, R.M., Webb, W.W.: Nonlinear magic: multiphoton microscopy in the biosciences. Nat. Biotechnol. **21**, 1369 (2003)
12. Yang, H.W., Hua, M.Y., Liu, H.L., Tsai, R.Y., Pang, S.T., Hsu, P.H., Tang, H.J., Yen, T.C., Chuang, C.K.: An epirubicin-conjugated nanocarrier with MRI function to overcome lethal multidrug-resistant bladder cancer. Biomaterials **33**, 3919 (2012)
13. Galeano Z, J.A., Sandoz, P., Gaiffe, E., Launay, S., Robert, L., Jacquot, M., Hirchaud, F., Pretet, J.L., Mougin, C.: Position-referenced microscopy for live cell culture monitoring. Biomed. Opt. Express **2**, 1307 (2011)
14. Barretto, R.P.J., Ko, T.H., Jung, J.C., Wang, T.J., Capps, G., Waters, A.C., Ziv, Y., Attardo, A., Recht, L., Schnitzer, M.J.: Time-lapse imaging of disease progression in deep brain areas using fluorescence microendoscopy. Nat. Med. **17**, 223 (2011)

15. Gorocs, Z., Ozcan, A.: On-chip biomedical imaging. IEEE Rev. Biomed. Eng. **6**, 29 (2013)
16. Fourkas, J.T.: Nanoscale photolithography with visible light. J. Phys. Chem. Lett. **1**, 1221 (2010)
17. Gross, H.N., Schott, J.R.: Application of spectral mixture analysis and image fusion techniques for image sharpening. Remote Sens. Environ. **63**, 85 (1998)